

AM of three-dimensional spongy microstructures for a piezoelectric sprayer

Chin-Tai Chen , Shin-Fang Hsu

Department of Mechanical Engineering, National Kaohsiung University of Science and Technology, Kaohsiung 80778, Taiwan
✉ E-mail: chintai@nkust.edu.tw

Published in Micro & Nano Letters; Received on 30th April 2018; Revised on 6th July 2018; Accepted on 9th August 2018

Additive manufacturing (AM) of spongy (cancellous) microstructures in the development and application of piezoelectric sprayers was investigated. The structures featuring microfluidic channels were made of solid polylactic acid (PLA) by fused deposition modelling (FDM) designed with a width of 35 mm, a depth of 25 mm, a height of 56 mm, and a cross-layer thickness of 2 mm. In total nine network structures were altered with the line widths (W_d) from 300 to 500 μm and the line spacing (S_d) from 250 to 400 μm . Then, one piezoelectric plate and another micronozzle array were assembled with the structures as a microactuator. The piezoelectric actuator had a resonance frequency of 107.8 ± 1 kHz, in which it generated microsprays of 3 ml water with a typical volumetric rate of ~ 1.1 ml/min. On the basis of FDM with PLA, the works' dimensional error analysis showed that the minimum AM errors ($<5\%$) between the design and actual dimensions occurred with the W_d of 350 μm and the S_d of 300–350 μm . In addition, they experimentally discovered anisotropic wettability and different roughness of the PLA layered surfaces, largely concerning the microfluidic performance of the network structures of the piezoelectric sprayer.

1. Introduction: Microsprays or droplets are of much interest over decades in the development of various applications such as inkjet printing [1] and spraying [2] for fabrication of thin films and microdevices [3–5]. The liquid of printing/spraying is normally stored in a reservoir containing sponges. Furthermore, based on conventional technologies of microelectro-mechanical systems, the fluidic flow can be continuously generated and transported in microscale using microactuators and channels. On the other hand, 3D-printed microfluidics [6] has been developed for the solid freeform fabrication of complex microstructures in three-dimensional (3D) state by exploring a variety of printing methods and materials [7, 8]. Among them, compared to other additive manufacturing (AM) techniques using ink and light [9–11], the fused deposition modelling (FDM) first developed by Crump [12] is frequently used for manufacturing process in recent research due to many advantages such as simple fabrication, high flexibility, low-cost, and eco-friendly materials [13–15]. Here, it is noted that the 3D manufacturing process of FDM in the previous work was mostly performed for the study of mechanical properties using polymer material such as polylactic acid (PLA) [16–18]. In addition, it was significantly applied for creation of scaffolds in the biomedical field of tissue engineering [19–22], featuring a 3D cellular network with high strength and porosity [23]. However, there is a little study on microfluidic properties incorporating with a mechatronic system for spongy networks, in which the capillary effect on storage and delivery of fluid capability play a significant role for the formation of droplets driven by electronic actuation. Failure in jetting droplets or absorbing liquid occurred without it. In this work, extended from our previous study on microspsays [24, 25], we designed and analysed the properties and characterisation of spongy microstructures for a microspsayer here. These porous structures exhibited similar cross-layered networks to each other but different line width and spacing (i.e. 250–500 μm) [26]. In this case, the line width (W_d) was designed together with a spacing of line (S_d) for AM of the microstructures. Therefore, different combinations of width and spacing within layers of structures permitted fluid to be delivered for generation of the microspsayer in distinct performances. It further benefits a variety of geometric designs applied to spray cooling [27], nanomaterial coating [28], microfluidic devices [29] etc.

2. Design and method

2.1. Configuration of a spongy structure: As illustrated in Fig. 1, a 3D porous network body (PNB) was designed with 3D of $W \times D \times H$ mm³ (i.e. width \times depth \times height) that features a spongy microstructure forming a number of pores (inner width of S and the outer width of C) in the interior of PNB. To examine whether this PNB can absorb and supply liquid as a reservoir, it would be further assembled with a piezoelectric actuator (PA) that is responsible for the generation of jetted droplets through a micronozzle array (MNA) using a piezoelectric ring [30, 31]. Using pure water as working fluid, we demonstrated for the first time how liquid is effectively transported over time simply by microfluidic actuation of water droplets (positive pressure) within the porous channels of the spongy microstructure (back pressure) [32].

The fluidic flow of water within the pores could be driven by the capillary force that exerts a Laplace's force $F_c = \gamma_{gl} \times \cos(\theta_{ls})/r$ on the free liquid–gas interface of porous channels, where γ_{gl} is the surface tension of solid–gas interface, θ_{ls} is the contact angle of liquid on solid, and r is the equivalent radius of curvature of the liquid–gas interface. Owing to the balance of capillary force with the gravity of the fluid, a maximum capillary height h can be expressed as below:

$$h = \frac{F_c}{\rho_l \times g} = \frac{\gamma_{gl} \times \cos(\theta_{ls})}{\rho_l \times g \times r} \quad (1)$$

where ρ_l is the density of liquid and g is the acceleration of gravity. For instance, g and r are the earth gravity of 9.8 m/s² and the pore radii between 150 and 250 μm , γ_{gl} is the surface tension of water in air (72 mN/m), θ_{ls} is the contact angle of water with PLA (60°), and ρ_l is the density of water (10³ kg/m³), respectively. Using (1), the capillary height for filling of liquid into the spongy structure was calculated to be 23–47 mm at maximum rise.

2.2. AM of cross-layered networks: To realise the complex microstructure of the PNB above, an AM method by FDM method is proposed as shown in Fig. 2. Using a filament roll of PLA driven by a delivery motor, the PNB can be 3D-printed layer by layer from bottom to top, in which each layer is perpendicularly separated (see Fig. 2a). In this way, individual PNB with 3D of $W \times D \times H$ can be straightforwardly manufactured as designed in Fig. 1. Then,

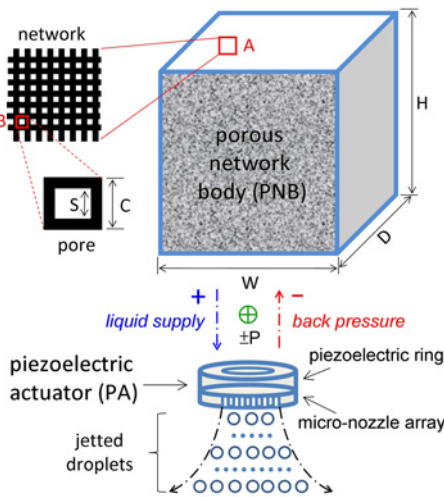


Fig. 1 Schematic configuration of a 3D PNB characterised with the inside of a network structure (see A) applied to contain and/or supply liquid for formation of jetted droplets from a fixed PA with a piezoelectric ring and an MNA. The PNB is with the width of W , the depth of D , and the height of H . Individual rectangular pore (see B) features the inner width of S and the outer width of C

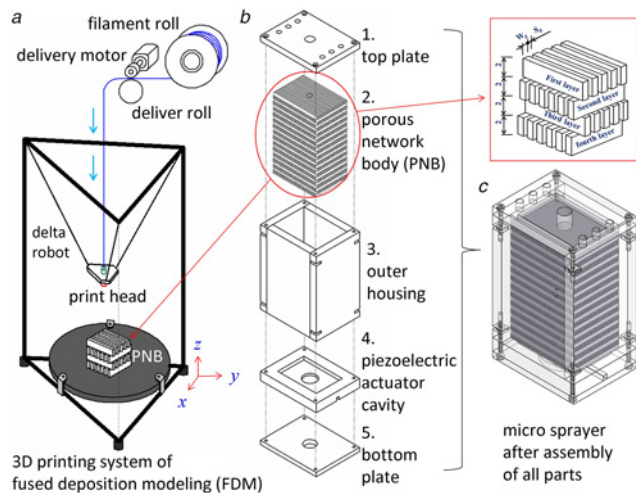


Fig. 2 Illustration of the AM process for the PNB assembled into a micro-sprayer including
a 3D printing system of FDM
b Five parts of the spray comprising the PNB (see red circle)
c Assembly of all the parts. Here, the FDM is carried out for the PNB with a 3D coordinate (x , y , and z) system, which corresponds to the schematic configuration of the studied 3D structure shown in Fig. 1

this PNB can be assembled with other packaging parts (i.e. top/bottom plates, outer housing, and PA cavity) made of conventional acrylic (see Fig. 2b), making it visible for observation in microfluidic experiment later. Finally, one microsprayer is simply produced after assembly of all parts (see Fig. 2c).

Furthermore, the void volume (V_{vo}) of the PNB, concerning the maximum content of liquid absorbed in volume, can be estimated by its amount of mass as $M_{PNB} = V_{so} \times \rho_{so} = (V_{PNB} - V_{vo}) \times \rho_{so}$, where V_{so} is the solid volume, ρ_{so} is the solid density of additive-manufactured material, and V_{PNB} is the outline volume of $W \times D \times H$. Through the correlation with the solid body, a porosity η corresponding to void percentage of the PNB can be expressed as follows:

$$\eta = (1 - \alpha) \times 100\% = 1 - \frac{V_{so}}{V_{PNB}} = 1 - \frac{M_{PNB}}{V_{PNB} \times \rho_{so}} \quad (2)$$

where α is the solid proportion of the PNB. Supposed that the 3D of $W \times D \times H$ are $35 \times 25 \times 56 \text{ mm}^3$ in the design of the PNB, thereby reaching the $V_{PNB} = 49 \text{ cm}^3$ for AM of PLA with the $\rho_{so} = 1.24 \times 10^3 \text{ kg/m}^3$. Using (2) with the mass of $M_{PNB} = 0.03 \text{ kg}$, for example, the solid content of α was estimated with -0.49 (i.e. nearby a half of the outline volume), thus leading to a porosity of $\eta = -51\%$ that allows it for maximum content (i.e. $-51\% \times 49 \text{ cm}^3 = 25 \text{ ml}$) of liquid absorbed within the porous body.

3. Experimental results

3.1. Production and tests of a spongy structure: On the basis of the above-mentioned design concept of FDM, a 3D model of the spongy structure was sliced with an infill parameter of 100% for generation of G-code (KISSlicer Com., USA). Then, it was directly produced using a 3D printer of ATOM 2.0 (Atom3dp Com., Taiwan) that permitted it to be printed with $\Phi 1.75 \text{ mm}$ (diameter) PLA filament by virtue of heating a print nozzle of $\Phi 350 \pm 50 \mu\text{m}$ (diameter) at 200°C . This printer was used for the production of PNB structures through the study. To probe the spongy function of PNB designed as a reservoir, it was followed by absorption of liquid water and tests of generation of microsperms with $\sim 1 \text{ ml/min}$ through ~ 1700 nozzles (each diameter $\Phi 6\text{--}7 \mu\text{m}$, pitch $\sim 300 \mu\text{m}$) of a PA (16 mm in outer diameter, $107 \pm 5 \text{ kHz}$ and DC 3–5 V, Whirl Best Int. Com., Taiwan) [27, 33]. Fig. 3 shows that the 3D-printed PNB was constructed under a layer thickness of $100 \mu\text{m}$ and a solid infill speed of $15\text{--}30 \text{ mm/s}$, exhibiting a volume $35 \times 25 \times 56 \text{ mm}^3$ with a typical height of 2 mm across each 20-layer stack (see Fig. 3a). Using a function generator (TDS 2012C, Tektronix, USA) connected to a microelectronic control unit (MCU) for tuning the resonant frequency appropriately (see Fig. 3b), a microsprayer with the PNB absorbing some water (see Fig. 3c) was demonstrated on a stage for generation of droplets (spray) by driving the actuator electrically (see Fig. 3d). Here, one inset in Fig. 3d illustrates the bottom of the PNB in tight contact with the PA, in which fluidic supply demanded such a spray was well-performed without leakage and shortage of water from PNB to PA [24, 25].

3.2. Influence of driving frequencies on sprays: As mentioned earlier, the PA should serve well for generating droplets with distributed sizes (i.e. a spray) through nozzles, if it is electrically

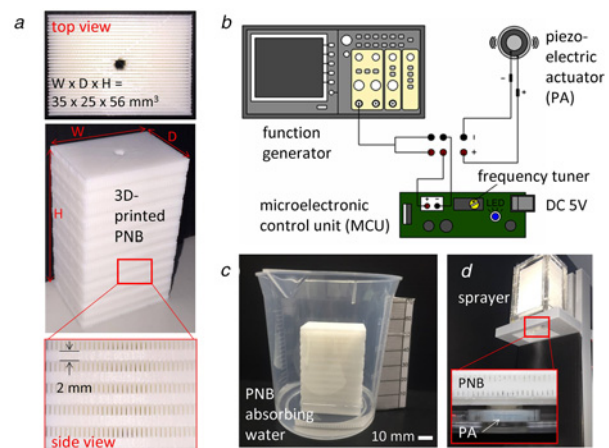


Fig. 3 Photography of experimental results with the
a 3D-printed production of the PNB sized with the width W of 35 mm, the depth D of 25 mm, and the height H of 56 mm
b Driving of the PA through a function generator and an MCU
c PNB absorbing water in a beaker
d Formation of jetted droplets with distributed sizes (a microspray) through the PA of the sprayer with a suitable driving frequency and voltage

driven at frequencies of 107 ± 5 kHz as specified by the manufacturer (Whirl Best Int.) [33]. However, as considering the assembly of the 3D-printed PNB with the actuator now, it is not clear about how the outcome of driving frequency affects the performance of sprays. To investigate the influence of driving frequency on volumetric rates of spray, the relationship between the driving frequencies and spraying time were investigated in this Letter. A wide range of frequencies from the function generator was fine tuned in the same matter to experimentally measure the time of sprays generated from the nozzles of the same PNB filled with liquid water of 3 ml (cm^3), as illustrated in Fig. 4a. Various amount of spray generation (i.e. water droplets jetted out of nozzles) was obtained ranging from 104 to 111 kHz, with a strong dependency on the frequency with spraying time approximately from 2 to 30 min. We attributed this result to the resonance of the piezoelectric system, in which the effective vibration generated from piezoelectric effect failed either below (104 kHz) or beyond (111 kHz) the specific bandwidth of $f_d = 107.5 \pm 3.5$ kHz.

Moreover, significant variance in the volumetric rate of spray was achieved simply by tuning the driving frequency (f_d). We measured and calculated the different volumetric rates of water spray for a total of ten frequencies (103.94–111.72 kHz). Fig. 4b illustrates the time and rate of spray at the specific bandwidth, where the rate was estimated from the total volume of 3 ml divided by time. We found that the volumetric rate obviously had a peak amount

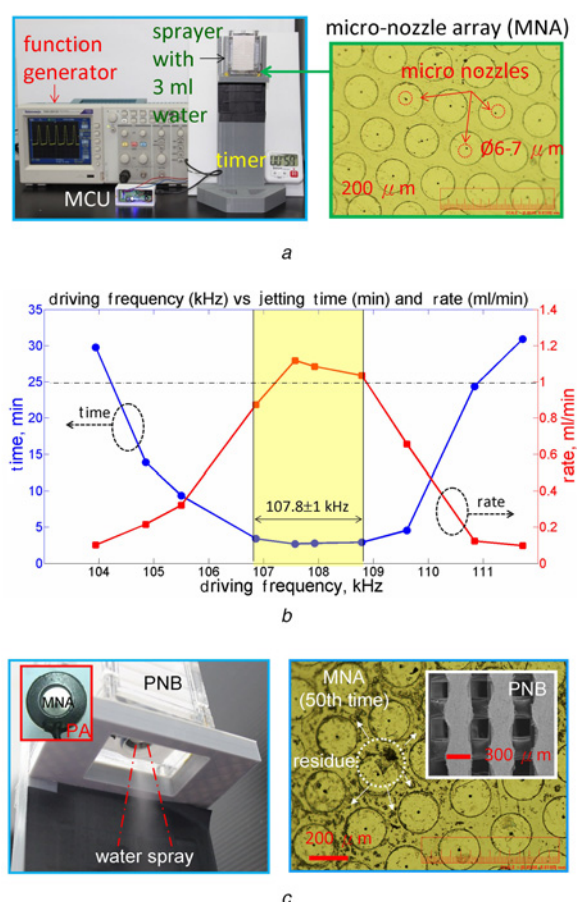


Fig. 4 Experimental setup and results for continuous formation of droplets jetted from the MNA of microsprayer under various driving frequencies
a Filling with water of 3 ml in volume, actuating via a function generator with MCU, and timing for calculation of volumetric rate
b Correlation among driving frequency, time, and rate demonstrating resonance frequencies of the piezoelectric sprayer at 107.8 ± 1 kHz
c Spray of water jetted from the MNA (nozzle diameter 6–7 μm) through the PNB leaving residues after multiple tests (50th time)

around 1.03–1.11 ml/min at frequencies nearby 107.8 ± 1 kHz. Increasing or decreasing the driving frequency from the peak resulted in a significant drop of the rate approaching 0.10–0.32 ml/min at 103.9–105.5 kHz and 0.10–0.66 ml/min at 109.6–111.7 kHz. This frequency-dependence qualitatively consists with theoretical work on piezoelectric sprayers [34]. In addition, the decrement of the rate of 0.55 ml/min (at 105.5 kHz) and 0.53 ml/min (at 110.8 kHz) occurred due to significant loss of pumping pressure within the PA cavity. It showed the maximum of volumetric rate around 1 ml/min at the resonant frequency of ~ 107 kHz, agreeing with those data measured for small diameters (5–7 μm) of nozzles [35]. The difference between the volumetric rates of present and previous work was attributed to the size, morphology, and properties of the material that affect the fluidic flow through the nozzles. Water residues arose from MNA after multiple tests, as shown in Fig. 4c but they were able to be cleaned to recover the performance with the removable PNB.

4. Analysis and discussion

4.1. Error analysis of microstructure dimensions: The dimensions of a 3D-printed PNB can be simply varied in width (W_d) and spacing (S_d) to analyse the accuracy of 3D printing on the networked microstructures through the present FDM using PLA. This analysis of error can be accomplished by comparing the 3D printing dimensions (actual results of W_a and S_a) with the designed ones (W_d and S_d). Fig. 5 demonstrates the error of 3D printing dimensions for a variety of W_d (see blue, 300–500 μm) and S_d (see red, 250–400 μm). In the total nine items with combinations of W_d (W) and S_d (S), it shows a common trend of dimensional errors: the positive deviation of W_a from W_d always resulted in the negative one of S_a from S_d and vice versa, implying that W_a plus S_a (e.g. No. 1: $656 \mu\text{m} + 197 \mu\text{m} = 853 \mu\text{m}$) approximately equals W_d plus S_d (e.g. No. 1: $500 \mu\text{m} + 350 \mu\text{m} = 850 \mu\text{m}$). Therefore, in the case of No. 4, as the actual width of $W_a = 351 \mu\text{m}$ approached the designed W_d of 350 μm , it also led to the smallest difference between the actual spacing ($S_a = 361 \mu\text{m}$) and designed value ($S_d = 350 \mu\text{m}$) by an error of -3.1% . Similar situation with minimal errors (absolute value $< 5\%$) was found in the case of No. 5. Both of them (Nos. 4 and 5) were corresponding to the print nozzle of 350 μm . This important result reveals a fundamental signature of the 3D printing based on FDM, in which the dimensional error of microstructures can be minimised as the design value agrees with the size of the print nozzle.

4.2. Surface roughness and capillary effect on the liquid: The surface roughness that affects the liquid water wetting on the

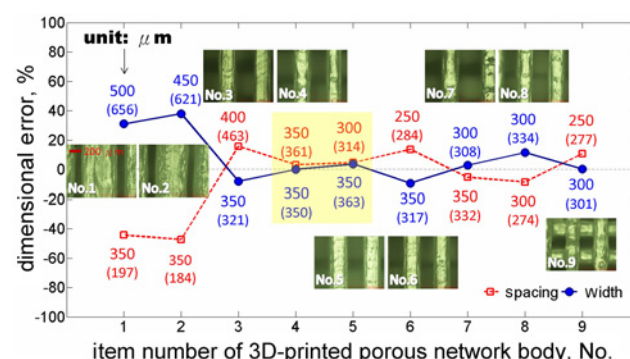


Fig. 5 Error analysis of 3D printing dimension of line width (W , blue solid line/circle) and spacing (S , red dash line/rectangle) for nine items printed (No. 1–9) using the FDM of PLA, in which the dimensions in design (width of W_d and spacing of S_d) are shown along with the actually measured ones (width of W_a and spacing of S_a) in parentheses. The printing dimensions of width and spacing ($W_d = 350 \mu\text{m}$, $S_d = 300$ – $350 \mu\text{m}$) with minimal errors ($< 5\%$) are highlighted in a yellow region

structure also depends on the layer thickness of 3D printing. This layer thickness can be adjusted simply by moving the print nozzle along the normal direction (i.e. z -axis in height) of the surface. In addition, anisotropic 2D surface roughness (R_a) might be resulted, since this 3D printing was completed using 1D filament of PLA. Fig. 6a demonstrates the different results on the top, bottom, and side surfaces using the layer thickness (t_L) of 50–300 μm . In the total six sets of representative measurement from a laser 3D profiler (resolution of 0.5 nm, VK-X260K, Keyence, JP), all roughness of the three surfaces (top, bottom, and side) showed a similar tendency of several-fold increase among $t_L = 50, 100$, and 150 μm , in which $R_a = 0.6\text{--}2.1\text{ }\mu\text{m}$ on top, 0.6–3.4 μm on bottom, and 4.7–11.6 μm on side. Eventually, it reached a maximum approximately beyond $t_L = 200\text{ }\mu\text{m}$, where $R_a = 2.2\text{ }\mu\text{m}$ (top), 3.8 μm (bottom), and 11.6 μm (side). The experimental results for all of the different thicknesses significantly indicate that the 3D-printed surface on the side was much rougher than the other surfaces using the present FDM method.

Moreover, this surface property produced by the FDM method was found to feature an anisotropic capillary effect of the liquid on the spongy structures. Fig. 6b illustrates a schematic diagram of hemi-spherical water drop wetting on the side surface, where the contact angle from side view 1 (i.e. θ_{S1} , perpendicular to the printing direction) is smaller than that from side view 2 (i.e. θ_{S2} , parallel with the printing direction). Using an analyser of contact angle (resolution of 0.1° , FTA-100, USA) for measurement of the produced surfaces, it showed the results of $\theta_{S1} = 61 \pm 1^\circ$ and $\theta_{S1} = 78 \pm 1^\circ$ on average of six sets, while the contact angle of $68 \pm 1^\circ$ was found on top. This minimum contact angle that occurred in the perpendicular direction of 3D printing further implied a dominant orientation of capillary flow. Hence, it suggests a useful rule of 3D printing design applicable to microfluidic flow

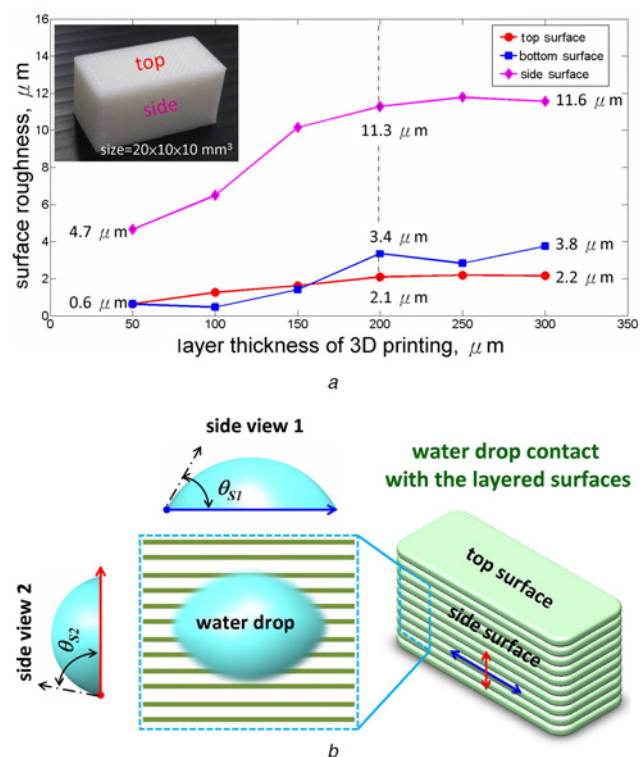


Fig. 6 Demonstration of the effect of 3D-printed layer thickness on surface roughness (0.6–11.6 μm) and wettability with water (e.g. contact angles θ_{S1} and θ_{S2})

a Experimental results of the surface roughness formed from different layer thicknesses (50–300 μm)

b Test of water drop contact with the surfaces generated from FDM process using PLA filaments

spontaneously delivered through microchannels generated by the FDM method in the future [6, 36, 37].

5. Conclusion: In summary, we presented an experimental study on AM of microsponty (cancellous) structures through solid PLA filament using FDM method. This Letter included the analysis and characterisation of a 3D PNB that allowed for a variety of line width (W : 300–500 μm) as well as a spacing (S : 250–400 μm) forming microfluidic channel network with a fixed volume of $35 \times 25 \times 56\text{ mm}^3$. Subsequently, the PNB was assembled with a PA to become a mechatronic system for controllable generation of micro water spray (1 ml/min at $\sim 107\text{ kHz}$). Further analysis of dimensional error and surface roughness demonstrates that the minimal error and roughness for FDM-based AM was $<5\%$ with the anisotropic feature, strongly depending on the 3D printing orientation. Those significant results would benefit the fundamental design and manufacturing of integrated devices using 3D printing in the microfluidic application in the future [38, 39].

6. Acknowledgments: The authors are grateful to the Department of Mechanical Engineering at the National Kaohsiung University of Science and Technology (former National Kaohsiung University of Applied Sciences) for access to major equipment of 3D printing and measurement.

7 References

- [1] Higuma M., Ikeda M., Sugama S., *ET AL.*: 'Ink filling method and apparatus for ink cartridge'. Patent No. 5790157, USA, 1998
- [2] Yu N.C.: 'Atomizing sprayer'. Patent Pub. No. 2015/0231660 A1, USA, 2015
- [3] Steirer K.X., Berry J.J., Reese M.O., *ET AL.*: 'Ultrasonically sprayed and inkjet printed thin film electrodes for organic solar cells', *Thin Solid Films*, 2009, **517**, pp. 2781–2786
- [4] Chen C.T.: 'Inkjet printing of microcomponents: theory, design, characteristics, and applications', in Kamanina N. (Ed.): 'Features of liquid crystal display materials and processes' (InTech, Rijeka, Croatia, 2011), pp. 43–60
- [5] Chen C.T.: 'Generation and evaporation of microsprints', in Yu X.Y. (Ed.): 'Advances in microfluidics – new applications in biology, energy, and materials sciences' (InTech, Rijeka, Croatia, 2016), pp. 315–334
- [6] Au A.K., Huynh W., Horowitz L.F., *ET AL.*: '3D-printed microfluidics', *Angew. Chem., Int. Ed.*, 2016, **55**, pp. 3862–3881
- [7] Wong K.V., Hernandez A.: 'A review of additive manufacturing', *ISRN Mech. Eng.*, 2012, **2012**, p. 208760
- [8] Chen C.T.: 'Microfabrication processes and applications of liquid photosensitive materials', in Tiwari A., Polykarpov A. (Eds.): 'Photocured materials' (RSC, Cambridge, UK, 2015), pp. 103–120
- [9] Compton B.G., Lewis J.A.: '3D-printing of lightweight cellular composites', *Adv. Mater.*, 2014, **26**, pp. 5930–5935
- [10] Zhu C., Han Y.J., Duoss E.B., *ET AL.*: 'Highly compressible 3D periodic graphene aerogel microlattices', *Nat. Commun.*, 2015, **6**, pp. 6962
- [11] Ventola C.L.: 'Medical applications for 3D printing: current and projected uses', *Pharm. Ther.*, 2014, **39**, pp. 704–711
- [12] Crump S.S.: 'Apparatus and method for creating three-dimensional objects'. Patent No. 5121329, USA, 1992
- [13] Guo S.Z., Gosselin F., Guerin N., *ET AL.*: 'Solvent-cast three-dimensional printing of multifunctional microsystems', *Small*, 2013, **9**, pp. 4118–4122
- [14] Lee W.C., Wei C.C., Chung S.C.: 'Development of a hybrid rapid prototyping system using low-cost fused deposition modeling and five-axis machining', *J. Mater. Process. Technol.*, 2014, **214**, pp. 2366–2374
- [15] Llewellyn-Jones T., Allen R., Trask R.: 'Curved layer fused filament fabrication using automated toolpath generation', *3D Print. Additive Manuf.*, 2016, **3**, pp. 236–243
- [16] Castilho M., Pires L., Gouveia B., *ET AL.*: 'Structural evaluation of scaffolds prototypes produced by three-dimensional printing', *Int. J. Adv. Manuf. Technol.*, 2011, **56**, pp. 561–569
- [17] Lanzotti A., Grasso M., Staiano G., *ET AL.*: 'The impact of process parameters on mechanical properties of parts fabricated in PLA

- with an open-source 3-D printer', *Rapid Prototyping J.*, 2015, **21**, (5), pp. 604–619
- [18] Lee J.Y., Tan W.S., An J., *ET AL.*: 'The potential to enhance membrane module design with 3D printing technology', *J. Membr. Sci.*, 2016, **499**, pp. 480–490
- [19] Hutmacher D.W.: 'Scaffolds in tissue engineering bone and cartridge', *Biomaterials*, 2000, **21**, pp. 2529–2543
- [20] Zein I., Hutmacher D.W., Tan K.C., *ET AL.*: 'Fused deposition modeling of novel scaffold architectures for tissue engineering applications', *Biomaterials*, 2002, **23**, pp. 1169–1185
- [21] Kalita S.J., Bose S., Hosick H.L., *ET AL.*: 'Development of controlled porosity polymer-ceramic composite scaffolds via fused deposition modeling', *Mater. Sci. Eng. C*, 2003, **23**, pp. 611–620
- [22] Hung K.C., Tseng C.S., Dai L.G., *ET AL.*: 'Water-based polyurethane 3D printed scaffolds with controlled release function for customized cartilage tissue engineering', *Biomaterials*, 2016, **83**, pp. 156–168
- [23] Bauer J., Hengsbach S., Tesari I., *ET AL.*: 'High-strength cellular ceramic composites with 3D microarchitecture', *Proc. Natl. Acad. Sci.*, 2014, **111**, pp. 2453–2458
- [24] Chen C.T., Wang H.Y.: 'Droplet generation and evaporative cooling using micro piezoelectric actuators with ring-surrounded circular nozzles', *Microsyst. Technol.*, 2015, **21**, pp. 2067–2075
- [25] Chen C.T., Huang C.C.: 'Microelectroforming and evaluation of honeycomb-groove nozzle plates of piezoelectric actuators for microspray', *J. Micro/Nanolithography MEMS MOEMS*, 2016, **15**, p. 035002
- [26] Sherrell P.C., Mattevi C.: 'Mesoscale design of multifunctional 3D graphene networks', *Mater. Today*, 2016, **19**, pp. 428–436
- [27] Hsieh S.S., Yeh Y.F., Li Y.F.: 'Microspray flow/thermal characteristics via a micro-piezoelectric atomizer with single and multiple arrays of micronozzles', *Exp. Therm. Fluid Sci.*, 2018, **93**, pp. 96–107
- [28] Munoz-Sandoval E., Fajardo-Diaz J.L., Sanchez-Salas R., *ET AL.*: 'Two sprayer CVD synthesis of nitrogen-doped carbon sponge-type nanomaterials', *Sci. Rep.*, 2018, **8**, p. 2983
- [29] Tsao C.W., Lei I.C., Chen P.Y., *ET AL.*: 'Piezo-ring-on-chip micro-fluidic device for simple and low-cost mass spectrometry interfacing', *Analyst*, 2018, **143**, pp. 981–988
- [30] Yan Q., Zhang J., Huang J., *ET AL.*: 'The effect of vibration characteristics on the atomization rate in a micro-tapered aperture atomizer', *Sensors*, 2018, **18**, p. 934
- [31] Hsieh S.S., Chang W.C.: 'Microspray quenching on nanotextured surfaces via a piezoelectric atomizer with multiple arrays of micronozzles', *Int. J. Heat Mass Transfer*, 2018, **121**, pp. 832–844
- [32] Song X., Zhu C., Fan D., *ET AL.*: 'A novel human-like collagen hydrogen scaffold with porous structure and sponge-like properties', *Polymers*, 2018, **9**, p. 638
- [33] Whirl Best Int. Com. Available at <http://www.whbest.com.tw>, accessed 5 July 2018
- [34] Zhong X., Lam S.: 'Perpetual-operation frequency response and equivalent circuit modeling of piezoelectric ultrasonic atomizer devices'. IEEE Int. Ultrasonics Symp. (IUS), Taipei, Taiwan, 2015
- [35] Chen H., Cheng W.L., Peng Y.H., *ET AL.*: 'Experimental study on optimal spray parameters of piezoelectric atomizer based spray cooling', *Int. J. Heat Mass Transfer*, 2016, **103**, pp. 57–65
- [36] Su W., Wu Z., Fang Y., *ET AL.*: '3D printed wearable flexible SIW and microfluidics sensors for Internet of things and smart health applications'. IEEE MTT-S Int. Microwave Symp. (IMS), HI, USA, 2017
- [37] Oomen P.E., Mulder J.P.S.H., Verpoorte E., *ET AL.*: 'Controlled, synchronized actuation of microdroplets by gravity in a superhydrophobic, 3D-printed device', *Anal. Chim. Acta*, 2017, **988**, pp. 50–57
- [38] Zhou Z., Cunningham E., Lennon A., *ET AL.*: 'Effects of poly (ϵ -caprolactone) coating on the properties of three-dimensional printed porous structures', *J. Mech. Behav. Biomed. Mater.*, 2017, **70**, pp. 68–83
- [39] Yang Y., Li X., Chen Z., *ET AL.*: '3D-printed biomimetic super-hydrophobic structure for microdroplet manipulation and oil/water separation', *Adv. Mater.*, 2018, **30**, p. 1704912